Journal of Renewable Materials

Tech Science Press

DOI: 10.32604/jrm.2022.022296

ARTICLE

Simulation Analysis of Stress Field of Walnut Shell Composite Powder in Laser Additive Manufacturing Forming

Yueqiang Yu[1], Tingang Ma[1], Suling Wang[1,*], Minzheng Jiang[1], Yanling Guo[2,3], Ting Jiang[1,*], Shuaiqi Huang[1], Ziming Zheng[1], Bo Yan[1] and Jiyuan Lv[1]

[1]College of Mechanical Science and Engineering, Northeast Petroleum University, Daqing, 163318, China

[2]College of Mechanical and Electrical Engineering, Northeast Forestry University, Harbin, 150040, China

[3]Research and Development Center of 3D Printing Material and Technology, Northeast Forestry University, Harbin, 150040, China

[*]Corresponding Authors: Suling Wang. Email: wangsuling@nepu.edu.cn; Ting Jiang. Email: jiangting1112@163.com

Received: 03 March 2022 Accepted: 04 May 2022

ABSTRACT

A calculation model of stress field in laser additive manufacturing of walnut shell composite powder (walnut shell/Co-PES powder) was established. The DFLUX subroutine was used to implement the moveable application of a double ellipsoid heat source by considering the mechanical properties varying with temperature. The stress field was simulated by the sequential coupling method, and the experimental results were in good accordance with the simulation results. In addition, the distribution and variation of stress and strain field were obtained in the process of laser additive manufacturing of walnut shell composite powder. The displacement of laser additive manufacturing walnut shell composite parts gradually decreased with increasing preheating temperature, decreasing laser power and increasing scanning speed. During the cooling process, the displacement of laser additive manufacturing of walnut shell composite parts gradually increased with the increasing preheating temperature, decreasing scanning speed and increasing laser power.

KEYWORDS

Selective laser sintering; agricultural and forestry wastes; walnut shell; stress field; warping deformation

1 Introduction

Additive manufacturing is considered as a rapid bottom-to-top free-form solid manufacturing technology that manufactures parts with complex geometric shapes by gradually adding materials to create three-dimensional entities, compared with subtractive manufacturing [1]. This technology can greatly reduce material waste and improve the research and development cycle of new products for manufacturing personalized parts. Meanwhile, it can also control the mechanical properties and microstructure of molded parts [2]. Selective Laser Sintering (SLS) was first proposed by Deckard [3]. It has the advantages of recyclable manufacturing materials, no need to add support structure, and fabricating parts of high molding accuracy [4]. Therefore, it is mainly used in aerospace [5], automotive parts [6], investment casting [7], biomedical engineering [8], and other industrial fields. However, the materials used in existing laser additive manufacturing technology are mostly metals [9], ceramics [10], polymers [11–13] and their composite powder materials [14–16], but rarely biomass composite powder

This work is licensed under a Creative Commons Attribution 4.0 International License, which permits unrestricted use, distribution, and reproduction in any medium, provided the original work is properly cited.

materials. Luckily, biomass composite powder materials are characterized by low cost, low power consumption, low processing conditions, stable manufacturing performance and fabricating small deformation parts. Therefore, it has great development potential [17].

At present, the biomass commonly used in laser additive manufacturing mainly includes rice husk [18], wood powder [19], bamboo powder [20], peanut shell [21] and other plant fibers. Compared with the above plant fibers, walnut shell is easy to be crushed and can easily reach the particle size required by laser additive manufacturing technology. Moreover, walnut shell powder particles are approximately spherical with good fluidity. Meanwhile, walnut shell powder is easy to be infiltrated by molten polymer and has good adsorption effect, which improves the binding effect of biomass fiber and polymer [22]. Therefore, walnut shell biomass fiber is selected as laser additive manufacturing material in this paper. However, in the laser additive manufacturing process, the high concentration and movement of laser heat source lead to uneven shrinkage of laser additive parts, and thermal stress result in warping or cracking of laser additive parts, which reduce the precision of laser additive parts. Due to the complexity of laser additive manufacturing process, the distribution and variation of stress field and displacement of additive parts in laser additive manufacturing process by experimental method are difficult to be obtained. Luckily, the finite element method can deal with this problem. Many studies are on the stress field of laser additive manufacturing of metal and ceramic materials [23–27], but few studies on the stress field of laser additive manufacturing non-metallic materials [28,29].

Hence, the finite element model of laser additive manufacturing walnut shell composite powder was established under the action of three-dimensional transient moving heat source and its stress field analyzed in this paper. The distribution and change law of stress and strain of laser additive manufacturing walnut shell composite powder was gained. The effect of processing parameters on displacement distribution and variation of laser additive manufacturing parts was studied, and their warping and cracking mechanism was discussed, in order to offer the theory sustain for laser additive manufacturing of forming parts.

2 Laser Additive Manufacturing Molding Process

The experiment is carried out in AFS-360 rapid prototyping sintering machine. The fast sintering machine is mainly composed of CO_2 laser, laser scanning system, temperature control system, powder supply system and powder distribution system, among which the rated laser power is 55 W, laser wavelength is 10.6 μm. The principle of laser additive manufacturing is to lay the powder on the powder bed by laying the roller, laser beam under the control of the computer, with a certain speed and energy in accordance with the cross-section CAD graphics of the 3D digital model for selective laser sintering of the powder bed, the roller will lay the powder on the sintered powder bed again, the laser beam is manufactured again according to the CAD pattern of the cross-section of the 3D digital model, and the cycle is repeated, using the principle of layering superposition, until the discrete accumulation of powder is manufactured into 3D solid parts, as shown in Fig. 1.

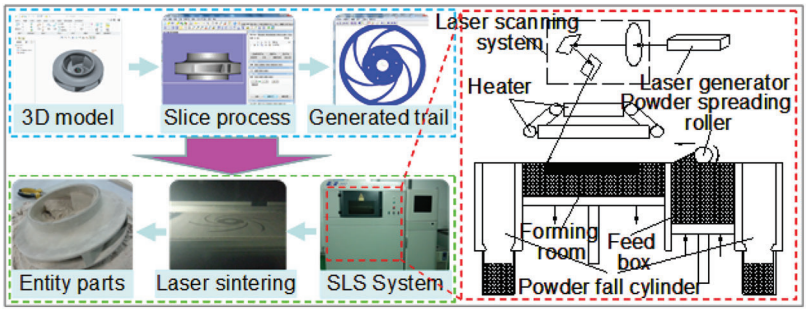

Figure 1: Forming principle of laser additive manufacturing walnut shell composite powder

3 Finite Element Numerical Simulation of Laser Additive Manufacturing

3.1 Stress Field Simulation Theory

In laser material in the manufacturing process, because the instantaneous laser radiation energy in laser additive manufacturing powder bed surface, make the powder bed surface laser radiation area temperature rising rapidly, and in other areas of the powder bed surface temperature did not alter, leading to large gradient of temperature field, laser additives stamping parts materials causing varying degrees of thermal expansion, the thermal stress will appear in the laser additive parts, and the thermal stress will inevitably lead to the warping deformation of the laser additive parts.

The equation of thermal deformation can be derived from Hooke's law, and its expression is as follows:

$$\begin{cases} \varepsilon_{xx} = \dfrac{1}{E}[\sigma_{xx} - v(\sigma_{yy} + \sigma_{zz})] + \alpha\tau = \dfrac{1}{2G}(\sigma_{xx} - \dfrac{v}{1+v}\Theta_s) + \alpha\tau \\ \varepsilon_{yy} = \dfrac{1}{E}[\sigma_{yy} - v(\sigma_{xx} + \sigma_{zz})] + \alpha\tau = \dfrac{1}{2G}(\sigma_{yy} - \dfrac{v}{1+v}\Theta_s) + \alpha\tau \\ \varepsilon_{zz} = \dfrac{1}{E}[\sigma_{zz} - v(\sigma_{xx} + \sigma_{yy})] + \alpha\tau = \dfrac{1}{2G}(\sigma_{zz} - \dfrac{v}{1+v}\Theta_s) + \alpha\tau \end{cases} \tag{1}$$

where E stands for the elastic modulus (Pa); v represents Poisson's ratio; α is coefficient of thermal expansion; τ is the amplitude of temperature change.

$$\Theta_s = \sigma_{xx} + \sigma_{yy} + \sigma_{zz} \tag{2}$$

$$\begin{cases} \varepsilon_{xy} = \dfrac{\sigma_{xy}}{2G} \\ \varepsilon_{yz} = \dfrac{\sigma_{yz}}{2G} \\ \varepsilon_{xz} = \dfrac{\sigma_{xz}}{2G} \end{cases} \tag{3}$$

$$\tau = T - T_0 \tag{4}$$

where T is temperature (K); T_0 is the initial temperature (K).

$$\varepsilon = \varepsilon_{xx} + \varepsilon_{yy} + \varepsilon_{zz} \tag{5}$$

where ε is the volumetric strain.

Eq. (1) can be deformed into:

$$\begin{cases} \sigma_{xx} = 2G\varepsilon_{xx} + \lambda\varepsilon - \dfrac{\alpha ET}{1-2v} \\ \sigma_{yy} = 2G\varepsilon_{yy} + \lambda\varepsilon - \dfrac{\alpha ET}{1-2v} \\ \sigma_{zz} = 2G\varepsilon_{zz} + \lambda\varepsilon - \dfrac{\alpha ET}{1-2v} \end{cases} \tag{6}$$

where G is shear elastic modulus, $G = E/2(1+v)$; λ is lame constant, $\lambda = vE/(1-2v)(1+v)$.

Eq. (3) can be deformed into:

$$\begin{cases} \sigma_{xy} = 2G\varepsilon_{xy} \\ \sigma_{yz} = 2G\varepsilon_{yz} \\ \sigma_{yz} = 2G\varepsilon_{yz} \end{cases} \tag{7}$$

3.2 Improved Double Ellipsoid Heat Source Model

In the process of laser additive manufacturing walnut shell composite powder, the laser radiation energy not only acts on the surface of the powder bed, but also acts on the depth of the powder bed through the gap between the powder particles. Therefore, the representative double ellipsoid heat source model is most suitable. Fig. 2a shows the double ellipsoid heat source model. DFLUX subroutine was used in the simulation process to realize the heat flux loading process, and Fig. 2b shows the loading path.

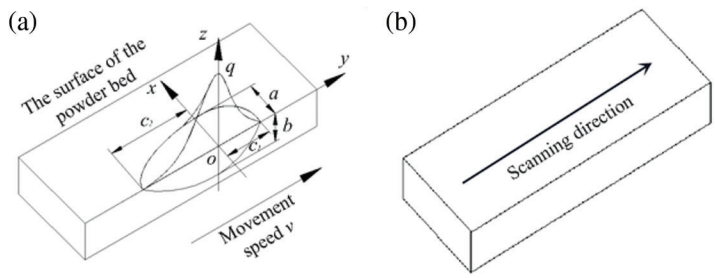

Figure 2: Double ellipsoid heat source model and trajectory control: (a) double ellipsoid heat source model; (b) trajectory control route. Adapted with permission from reference [30]. Copyright © 2021. Elsevier

The double ellipsoid heat source model contains two different 1/4 ellipsoids, and the heat flux distribution in the rear and front ellipsoids are different. The heat flux equation of the front and rear ellipsoids are as follows:

$$q(x,y,z,t) = \frac{6\sqrt{3}\eta f_f Q}{abc_1\pi\sqrt{\pi}} e^{\frac{-3x^2}{a^2}} e^{\frac{-3[y+v(\tau-t)^2]^2}{c_1^2}} e^{\frac{-3z^2}{b^2}} \tag{8}$$

$$q(x,y,z,t) = \frac{6\sqrt{3}\eta f_r Q}{abc_2\pi\sqrt{\pi}} e^{\frac{-3x^2}{a^2}} e^{\frac{-3[y+v(\tau-t)^2]^2}{c_2^2}} e^{\frac{-3z^2}{b^2}} \tag{9}$$

where c_1 stands for the first half axis (m) in the Y direction; c_2 represents the rear half axis (m) in the Y direction; a stands for the semi-major axis (m) in the X direction; b represents the semi-major axis (m) in the Z direction; η is the powder absorption rate; Q represents the laser power (W); t represents the heat source action time (s); v represents the heat source movement velocity (m/s); τ represents the time delay factor; f_f and fr are the energy distribution coefficients of the front and rear ellipsoids respectively, $f_f + f_r = 2$.

In the process of walnut shell composite powder laser additive manufacturing, due to the use of laser heat source, $c_1 = c_2 = c = a$, so $f_f = f_r = 1$. The power density distribution function of the improved double ellipsoid heat source model:

$$q(x,y,z,t) = \frac{6\sqrt{3}\eta Q}{abc\pi\sqrt{\pi}} e^{\frac{-3x^2}{a^2}} e^{\frac{-3[y+v(\tau-t)^2]^2}{c^2}} e^{\frac{-3z^2}{b^2}} \tag{10}$$

where, c is semi-major axis (m) in the Y direction.

The laser beam will produce a "semicircular" sintering pool on the powder bed [31]. It is also known that the absorption rate η of the walnut shell composite powder material by the CO_2 laser beam is 0.96. The laser spot diameter is 0.0004 m. Therefore, if $a = b = c = 0.0002$ m. The single layer thickness by laser additive manufacturing experiment and powder bed surface temperature thermal maps by FLUKE Ti400 infrared thermal imaging instrument were compared with the finite element temperature field simulation results, and the values were basically consistent (deviation within 5%), so the selected heat source parameters were reasonable [30].

3.3 Stress Field Simulation Model is Established

3.3.1 Finite Element Model

It is impossible to use two-dimensional model to describe the sintering area of powder bed, because the energy absorbed by powder bed is different in X, Y and Z directions. Hence, establishing a three-dimensional finite element geometric model in a must on the basis of the actual situation of laser additive manufacturing walnut shell composite powder. However, the calculation efficiency of the model will be affected if the model is built completely according to the actual situation. Therefore, in the context of comprehensive consideration of calculation accuracy and efficiency, this paper simplified the finite element geometric model of walnut shell composite powder, and the simplified model size: 3.2 mm × 1.2 mm × 0.3 mm, as shown in Fig. 3a. In the process of stress field simulation of laser additive manufacturing walnut shell composite powder, the finite element model used is a simple cuboid. Therefore, the three dimensional stress structure element C3D8R was used to conduct mesh division for the three dimensional finite element geometric model of walnut shell composite powder. The mesh density of laser heat source area and other areas was 0.05 mm. Fig. 3b shows the segmented finite element mesh model.

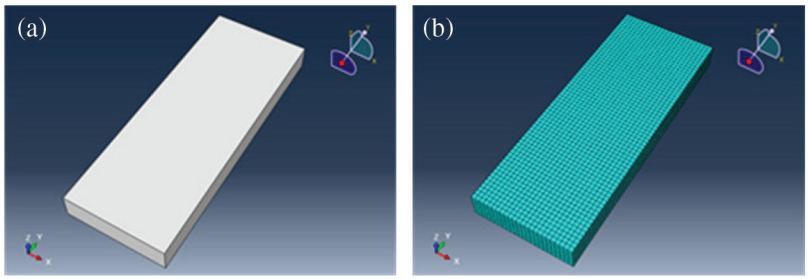

Figure 3: Three-dimensional finite element geometric model and mesh model of walnut shell composite powder: (a) three-dimensional finite element geometric model; (b) finite element mesh model. Adapted with permission from reference [30] Copyright © 2021. Elsevier

3.3.2 Initial and Boundary Conditions

Due to the thermal expansion coefficient between different objects contacting each other or different parts of the same object, the expansion or contraction degree of each other is not consistent when the objects are heated or cooled, which is easy to produce thermal stress. The laser beam instantaneous action on the powder bed, so that the powder temperature in the radiation area rose rapidly, and the surrounding powder produced a large temperature gradient, from the thermal stress. Temperature field and thermal stress reaction to that influence temperature field distribution and change, because the laser material in the manufacturing process, the thermal stress of walnut shell composite powder laser material manufacturing has little effect on temperature field, so this article choose sequence coupling method of walnut shell composite powder laser material manufacturing stress field is analyzed, Fig. 4 shows its analysis process.

As the stress field simulation adopts the sequential thermodynamic coupling method, the author has solved the temperature field and obtained the calculation results of the temperature field [31]. According to the actual forming conditions, the initial temperature was first set at 80°C, and then the calculated results of the initial temperature and temperature field were loaded to the nodes of the model as temperature loads. As for the constraints of the model, the center position of the bottom surface of the model is constrained by the cross form, and then the translational and rotational degrees of freedom of the model X, Y and Z are equivalent constrained. Boundary conditions are set as shown in Fig. 5.

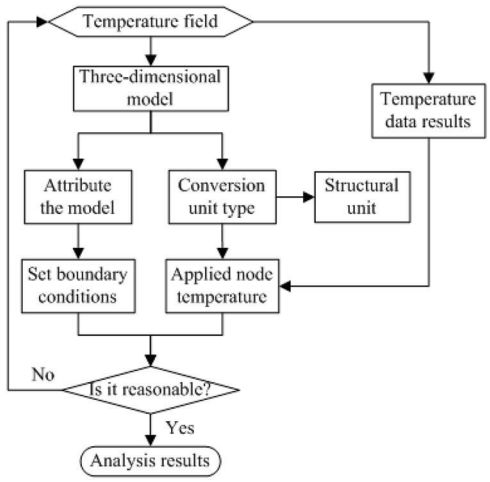

Figure 4: Flow chart of sequential coupling analysis

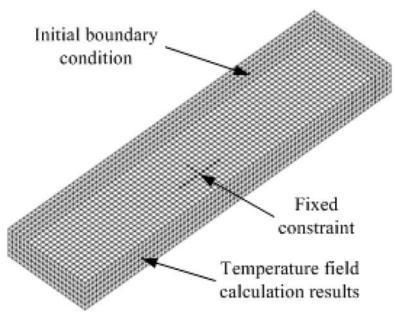

Figure 5: Load and boundary conditions

3.3.3 Computational Model Attributes

Because the laser additive manufacturing process of walnut shell composite powder is a rapid solidification process and melting process. The mechanical properties of the material will change nonlinearly in this process. Therefore, the elastic modulus, yield strength and thermal expansion coefficient of materials are particularly important. The mechanical property parameters of the walnut shell composite powder laser additive were tested, and the elastic modulus and yield strength varied with temperature were obtained, as well as the thermal expansion coefficient and Poisson's ratio. Table 1 shows the specific mechanical property parameters.

Table 1: Mechanical properties of walnut shell composites

Temperature (°C)	20	30	40	50	60	110
Modulus of elasticity (MPa)	699.5	385.7	180.1	99.02	71.25	0.8787
The yield strength (KPa)	326.2	182.6	83.47	46.31	33.27	0.417
Coefficient of thermal expansion (10^{-5}/°C)	3.82					
Poisson's ratio	0.35					

3.4 Simulation Verification of Stress and Strain Field of Laser Additive Parts

With laser power of 10 W, scanning speed is 1.8 m/s, preheating temperature is 80°C, layering thickness of 0.1 mm, technology parameters of the scanning interval is 0.2 mm for laser additive manufacturing test and stress field simulation test, for walnut shell composite powder laser material gain the actual deformation condition and the simulation of parts in Fig. 6. Fig. 6a shows that there is no obvious warping deformation in the center of laser additive manufacturing walnut shell composite parts, and the warping deformation becomes more and more obvious from the center to both ends. Fig. 6b is the simulation deformation result. Since the deformation is small in the thickness direction, it is not easy to observe the deformation trend, so it is magnified by 100 times. The simulation deformation after magnified by 100 times is shown in Fig. 6c. the warping deformation trend of laser additive manufacturing walnut shell composite parts is roughly the same. Therefore, the analysis results of stress field in the simulation process of laser additive manufacturing walnut shell composite powder are reasonable.

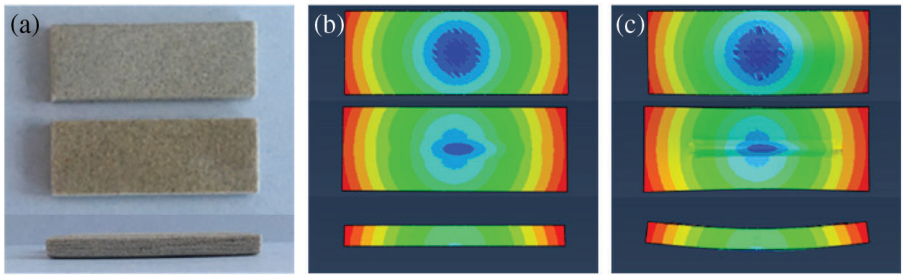

Figure 6: Comparison between simulation deformation and actual deformation results of laser additive parts: (a) actual deformation; (b) simulation deformation (c) simulation deformation with magnification 100 times

4 Results and Discussion

4.1 Stress and Strain Distribution of Walnut Shell Composite Powder Additive Manufacturing Process

Fig. 7 shows the stress and strain distribution at the mid-point of laser scanning track at t = 0.0006 s under preheating temperature of 80°C, laser power of 10 W and scanning speed of 2 m/s. In order to facilitate the observation of stress-strain changes, the scaling coefficient of the stress-strain cloud image was set to 100 times. Figs. 7a–7c show that the protrusion of material in the laser action area is significantly higher than the height of the material in the unsintered area, and its equivalent stress is very small, about 0 KPa. This is mainly because of the effect of laser radiation, the material absorbs heat and the temperature rises rapidly, resulting in the expansion deformation of the material when heated. When the material melts into the liquid phase, the material is in a plastic state, so the equivalent stress is 0 KPa. The overall stress in the laser scanning area is tensile stress, which is about 0.998 KPa. When the laser beam is far away, the temperature of the material in the sintering area declines, which leads to the shrinkage of the material when it cools, while the material with lower temperature around prevents its shrinkage, thus producing tensile stress. The stress in scanning direction and the stress in vertical scanning direction are different, the scanned area in scanning direction is mainly tensile stress, the smaller compressive area is near the sintering pool, and scanned area in vertical scanning direction is mainly compressive stress, and the maximum stress difference between two scanning areas is large, the maximum stress in the scanning direction is about 1.448 KPa, and the maximum stress in the vertical scanning direction is about 0.67 KPa. Due to the large stress in scanning direction, the deformation of laser additive parts in scanning direction is large, while the stress distribution gradient in vertical scanning direction is large, which easily causes defects such as cracks in laser additive parts. Fig. 7d shows that the plastic strain distribution of the material is related to the equivalent stress distribution to a certain extent. The plastic strain of the material in the center of the laser

beam is the largest and gradually decreases to both sides. The main reason is that the energy in the center of laser beam is the highest, gradually decreasing to both sides, so that the most heat is absorbed by materials in the center of laser beam, thus its temperature is the highest.

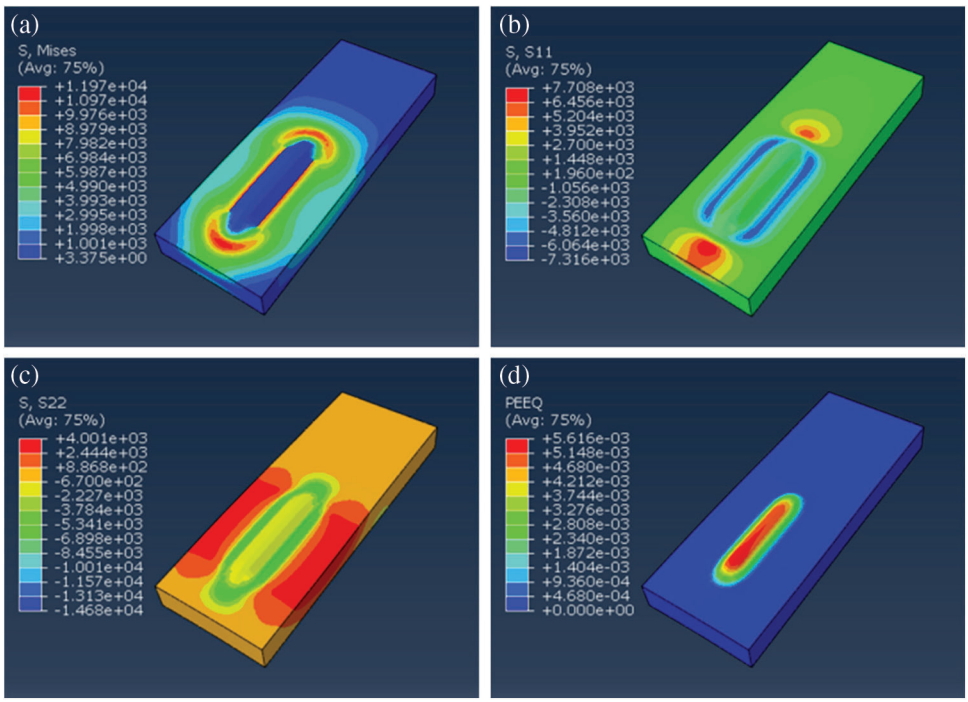

Figure 7: Distribution cloud images of instantaneous stress and strain field in laser additive manufacturing walnut shell composite powder: (a) equivalent stress; (b) stress in the scanning direction; (c) stress in vertical scanning direction; (d) equivalent plastic strain

4.2 Effect of Preheating Temperature on Displacement Distribution and Variation of Laser Additive Parts

Fig. 8 shows the displacement distribution and change curves of laser additive parts at different preheating temperatures (76°C, 78°C, 80°C, 82°C, 84°C) with scanning speed of 2 m/s and laser power of 10 W. It can be seen from Figs. 8a–8e that the displacement of the central region of the laser additive manufacturing walnut shell composite parts is 0 m, which presents an uneven gradient distribution to both ends of the laser additive manufacturing walnut shell composite parts and the displacement of parts gradually increases. The displacement of the two ends of the walnut shell composite powder laser additive is the largest. By the increase of preheating temperature, the displacement distribution of walnut shell composite laser additive parts has no obvious change, the displacement of the central region is still 0 m, and the displacement of the two ends of the region increases gradually. Fig. 8f shows the displacement variation curve of laser additive parts during the whole analysis process, which includes processing and cooling processes, and the analysis time is set at 0.0012 and 500 s, respectively. Fig. 8g demonstrates the displacement variation curve during processing, while Fig. 8h demonstrates that during cooling. It can be seen from Figs. 8f–8h that when the preheating temperature rises from 76°C to 84°C, the displacement of the laser additive manufacturing walnut shell composite parts gradually decreases in the processing process, and increases gradually in the cooling process. The main reason is that when the scanning speed and laser power are unchanged, the bed preheating temperature is low, the laser input energy is high, the surface of the bed is easy to produce a large temperature gradient, so that the displacement of the laser additive parts increases. With increasing preheating temperature, the surface temperature gradient of powder bed decreases gradually, so the displacement of laser additive parts

decreases gradually. In the cooling process, along with the increasing heat which the preheating temperature of powder bed absorbs, the internal heat of laser additive parts increases, laser additive parts temperature is higher, when the temperature of the laser additive parts is reduced to room temperature, the temperature difference of laser additive parts increases, leading to an increasing displacement of laser additive parts.

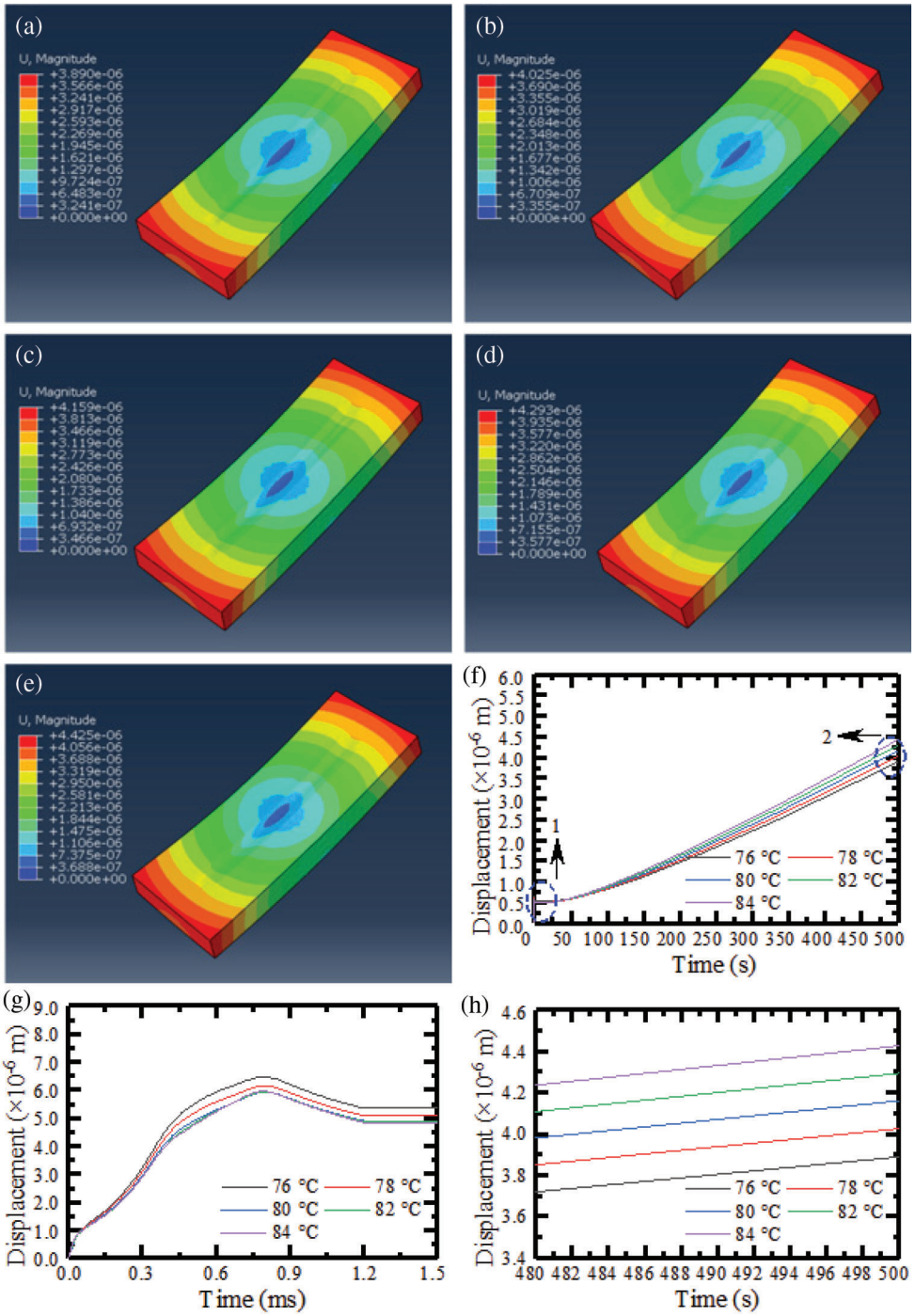

Figure 8: Displacement distribution and variation curves of laser additive parts with different preheating temperatures: (a) 76°C; (b) 78°C; (c) 80°C; (d) 82°C; (e) 84°C; (f) the curves of displacement; (g) A larger version of position 1 (h) A larger version of position 2

4.3 Effect of Laser Power on Displacement Distribution and Variation of Laser Additive Parts

In Fig. 9, the displacement distribution and change curves of laser additive parts under different laser powers (8, 10, 12, 14 and 16 W) at preheating temperature of 80°C and scanning speed of 2 m/s. It can be seen from Figs. 9a–9e that the displacement of the central region of the laser additive manufacturing walnut shell composite parts is 0 m, which presents an uneven gradient distribution to both ends of parts and the displacement gradually increases, especially the displacement of the two ends of parts is the largest. With increasing laser power, the displacement distribution of laser additive manufacturing walnut shell composite parts has no obvious change, the displacement of the central region is still 0 m, and the displacement of the two ends gradually increases. Fig. 9f demonstrates the displacement variation curve of laser additive parts during the whole analysis process, which includes processing and cooling processes, and the analysis time is set at 0.0012 and 500 s, respectively. Fig. 9g demonstrates the displacement variation curve during processing, while Fig. 9h shows that during cooling. In Figs. 9f–9h, the laser power increasing from 8 to 16 W, the displacement of the laser additive manufacturing walnut shell composite parts gradually increases in the processing process, and also in the cooling process. The main reason is that in the process of processing, when the preheating temperature and scanning speed is constant, the laser power is small, the energy input of the laser is less, the energy absorbed by the powder bed is less, the surface temperature gradient of the powder bed is smaller, so the displacement of the laser additive parts is smaller. With increasing laser power, the more energy absorbed by the powder bed, the larger the surface temperature gradient of the powder bed, leading to larger the displacement of the laser additive parts. In the cooling process, with increasing laser power, heat which powder bed absorbs increases gradually, so the temperature of laser additive parts becomes high. When the temperature of the laser additive parts is reduced to room temperature, the temperature difference of laser additive parts increases, leading to the increasing displacement of laser additive parts.

4.4 Effect of Scanning Speed on Displacement Distribution and Variation of Laser Additive Part

Fig. 10 shows the displacement distribution and change curve of laser additive manufacturing walnut shell composite parts at different scanning speeds (1.4, 1.6, 1.8, 2.0, 2.2 m/s) with laser power of 10 W, preheating temperature of 80°C. As can be seen from Figs. 10a–10e, the displacement of the central region of the laser additive manufacturing walnut shell composite parts is 0 m, and the displacement of the two ends is the largest, and presents an uneven gradient distribution from the center to the two ends, and the displacement gradually increases. With rising scanning speed, the displacement distribution of laser additive manufacturing walnut shell composite parts has no obvious change, the displacement of the central region is still 0 m, but the displacement of the two ends of the region gradually decreases. Fig. 10f demonstrates the displacement variation curve during the whole analysis process, which includes processing and cooling processes, and the analysis time is set at 0.0012 and 500 s, respectively. Fig. 10g demonstrates the displacement variation curve during processing, while Fig. 10h demonstrates that during cooling. As can be seen from Figs. 10f–10h, when the scanning speed rising from 1.4 to 2.2 m/s, the displacement of the laser additive manufacturing walnut shell composite parts decreases gradually during processing and cooling. The main reason is that when preheating temperature and laser power are fixed, slow scanning speed leads to more laser energy absorbed by the powder bed, and the higher temperature results in the greater temperature gradient generated on the surface of the bed, so that the displacement of the laser additive parts increases. With the increase of scanning speed, the absorbed laser energy decreases and the temperature gradient of the powder bed surface decreases, so the displacement of the laser additive parts decreases gradually. In the cooling process, along with the increase of the scanning speed, the absorbed heat is gradually reduced, the heat inside the laser additive parts declines, and the temperature of the laser additive parts is gradually reduced. When the temperature of the laser additive parts is reduced to room temperature, the temperature difference of the laser additive parts is reduced, resulting in a reduced displacement of the laser additive parts.

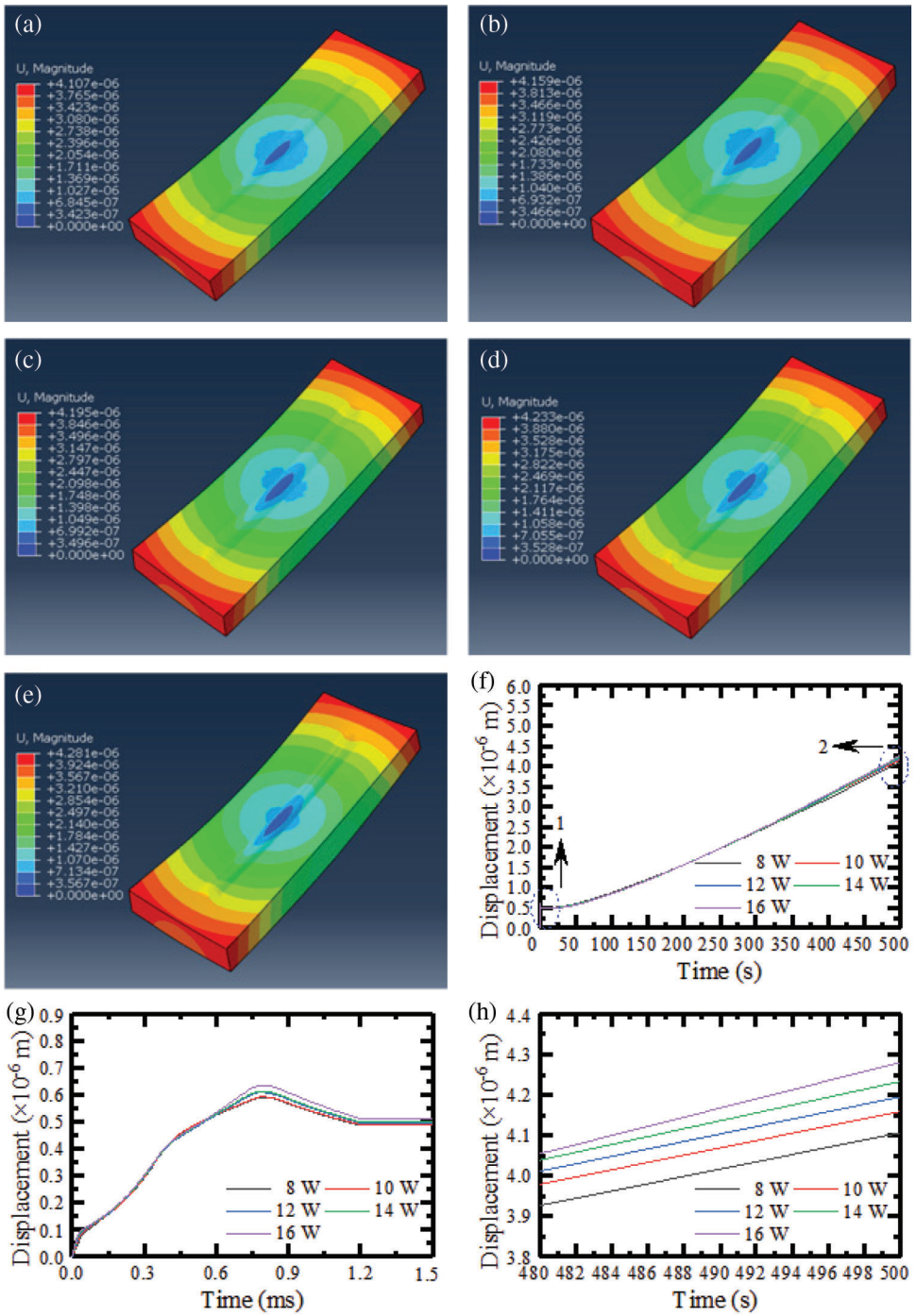

Figure 9: Displacement distribution and variation curves of laser additive parts under different laser powers: (a) 8 W; (b) 10 W; (c) 12 W; (d) 14 W; (e) 16 W; (f) Displacement change curve; (g) A larger version of position 1; (h) A larger version of position 2

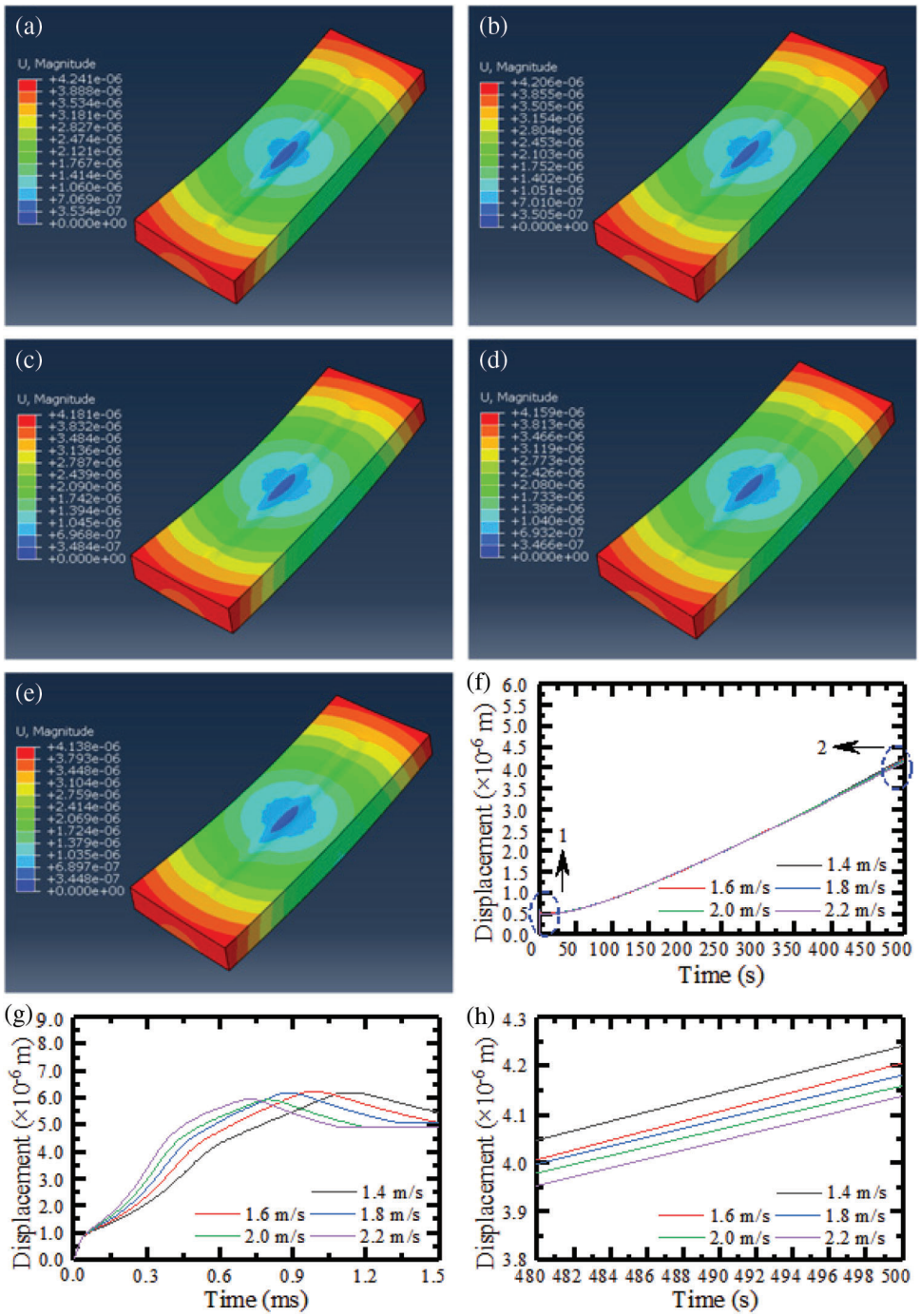

Figure 10: Displacement distribution and variation curves of laser additive parts at different scanning speeds: (a) 1.4 m/s; (b) 1.6 m/s; (c) 1.8 m/s; (d) 2.0 m/s; (e) 2.2 m/s; (f) Displacement curve; (g) A larger version of position 1; (h) A larger version of position 2

5 Conclusions

1. Based on the physical process of laser additive manufacturing, the double ellipsoid heat source model was improved to enhance the adaptability of the existing heat source model to the simulation of laser additive manufacturing walnut shell composite powder, so as to effectively improve the numerical simulation accuracy of stress field.
2. There was no obvious warping deformation in the center of the laser additive manufacturing walnut shell composite parts by comparative analysis of numerical simulation and experiment, and the warping deformation becomes more and more obvious from the center to both ends. Compared with the simulation results, the warping deformation was smaller, but the warping deformation trend of the laser additive manufacturing walnut shell composite parts was roughly the same. Therefore, the numerical simulation results of stress field of laser additive manufacturing forming process are reasonable.
3. The stress field of laser additive manufacturing walnut shell composite powder was numerically simulated by using the improved double ellipsoid heat source model, and the strain and stress distribution and variation law of laser additive parts were obtained. The displacement of laser additive parts gradually decreased with increasing preheating temperature, increasing scanning speed and decreasing laser power. During the cooling process, the displacement of laser additive parts gradually enlarges by increasing preheating temperature, increasing laser power and decreasing scanning speed.

Data Availability Statement: The data that support the findings of this study are available from the corresponding authors upon reasonable request.

Funding Statement: Supported by the Scientific Research Start-Up Fund Project of Northeast Petroleum University (2019KQ67 and 2021KQ09), the Guiding Innovation Fund Project of Northeast Petroleum University (2021YDL-13), National Natural Science Foundation of China (52075090), and Supported by the National Key R&D Program of China (2017YFD0601004).

Conflicts of Interest: The authors declare that they have no conflicts of interest to report regarding the present study.

References

1. Bahnini, I., Rivette, M., Rechia, A., Siadat, A., Elmesbahi, A. (2018). Additive manufacturing technology: The status, applications, and prospects. *The International Journal of Advanced Manufacturing Technology, 97(1–4),* 147–161. DOI 10.1007/s00170-018-1932-y.
2. Westerweel, B., Basten, R., Houtum, G. (2018). Traditional or additive manufacturing? Assessing component design options through lifecycle cost analysis. *European Journal of Operational Research, 270(2),* 570–585. DOI 10.1016/j.ejor.2018.04.015.
3. Deckard, C. R. (1988). *Selective laser sintering (Ph.D. Thesis)*. The University of Texas at Austin, USA.
4. Gross, B. C., Lockwood, S. Y., Spence, D. M. (2016). Recent advances in analytical chemistry by 3D printing. *Analytical Chemistry, 89(1),* 57–70. DOI 10.1021/acs.analchem.6b04344.
5. Zhang, H., Dong, D., Su, S., Chen, A. (2019). Experimental study of effect of post processing on fracture toughness and fatigue crack growth performance of selective laser melting Ti-6Al-4V. *Chinese Journal of Aeronautics, 32(10),* 2383–2393. DOI 10.1016/j.cja.2018.12.007.
6. Wang, D., Wang, Y., Yang, Y., Lu, J., Zhang, D. (2019). Research on design optimization and manufacturing of coating pipes for automobile seal based on selective laser melting. *Journal of Materials Processing Technology, 273(2),* 116227. DOI 10.1016/j.jmatprotec.2019.05.008.

7. Yang, L., Tang, S. Y., Fan, Z. T., Jiang, W. M., Liu, X. W. (2021). Rapid casting technology based on selective laser sintering. *China Foundry, 18(4),* 296–306. DOI 10.1007/s41230-021-1099-2.
8. Kamboj, N., Ressler, A., Hussainova, I. (2021). Bioactive ceramic scaffolds for bone tissue engineering by powder bed selective laser processing: A review. *Materials, 14(18),* 5338. DOI 10.3390/ma14185338.
9. Li, Z. H., Teng, B. R., Yao, B. B., Liu, J. (2021). Microstructure and mechanical properties of WC reinforced 18Ni300 composites produced by selective laser melting. *Materials Characterization, 180,* 111406. DOI 10.1016/j.matchar.2021.111406.
10. Wang, K. J., Bao, C. G., Zhang, C. Y., Li, Y. H., Liu, R. Z. et al. (2021). Preparation of high-strength Si_3N_4 antenna window using selective laser sintering. *Ceramics International, 48(2),* 2903–2911. DOI 10.1016/j.ceramint.2021.09.307.
11. Czelusniak, T., Amorim, F. L. (2021). Influence of energy density on polyamide 12 processed by SLS: From physical and mechanical properties to microstructural and crystallization evolution. *Rapid Prototyping Journal, 27(6),* 1189–1205. DOI 10.1108/RPJ-02-2020-0027.
12. Shuai, C. J., Xu, Y., Feng, P., Wang, G. Y., Xiong, S. X. et al. (2019). Antibacterial polymer scaffold based on mesoporous bioactive glass loaded with *in situ* grown silver. *Chemical Engineering Journal, 374(22),* 304–315. DOI 10.1016/j.cej.2019.03.273.
13. Shuai, C. J., Liu, G. F., Yang, Y. W., Qi, F. W., Peng, S. P. et al. (2020). A strawberry-like Ag-decorated barium titanate enhances piezoelectric and antibacterial activities of polymer scaffold. *Nano Energy, 74,* 104825. DOI 10.1016/j.nanoen.2020.104825.
14. Jucan, O. D., Gădălean, R. V., Chicinaş, H. F., Hering, M., Bâlc, N. et al. (2021). Study on the indirect selective laser sintering (SLS) of WC-Co/PA12 powders for the manufacturing of cemented carbide parts. *International Journal of Refractory Metals and Hard Materials, 96,* 05498. DOI 10.1016/j.ijrmhm.2021.105498.
15. Pelanconi, M., Colombo, P., Ortona, A. (2021). Additive manufacturing of silicon carbide by selective laser sintering of PA12 powders and polymer infiltration and pyrolysis. *Journal of the European Ceramic Society, 41(10),* 5056–5065. DOI 10.1016/j.jeurceramsoc.2021.04.014.
16. Lupone, F., Padovano, E., Ostrovskaya, O., Russo, A., Badini, C. (2021). Innovative approach to the development of conductive hybrid composites for selective laser sintering. *Composites Part A: Applied Science and Manufacturing, 147,* 106429. DOI 10.1016/j.compositesa.2021.106429.
17. Guo, Y. L., Jiang, K. Y., Yu, Z. X., Xin, Z. S., Zeng, W. L. (2011). The preparation technology and forming properties of wood-plastic composite powder used in selective laser sintering. *Journal of Shanghai Jiaotong University, 45(9),* 1327–1331. DOI 10.1002/clc.20818.
18. Zeng, W. L., Guo, Y. L., Jiang, K. Y. (2012). Preparation and selective laser sintering of rice husk-plastic composite powder and post processing. *Digest Journal of Nanomaterials & Biostructures, 7(3),* 1063–1070.
19. Zhang, Y., Wang, F., Zhang, Y., Li, J., Guo, Y. (2021). Effect of al powder on mechanical properties and microstructure of wood-plastic composites by selective laser sintering. *Materials Today Communications, 27,* 102235. DOI 10.1016/j.mtcomm.2021.102235.
20. Guo, Y. L., Jiang, K. Y., Zhang, H., Zhao, D. J. (2017). Preparation and selective laser sintering of bamboo flour/copolyester composite and post-processing. *Journal of Thermoplastic Composite Materials, 30(8),* 1045–1055. DOI 10.1177/0892705715616854.
21. Idriss, A., Li, J., Guo, Y. L., Wang, Y. E., Ahmed, A. I. B. (2021). Improved sintering quality and mechanical properties of peanut husk powder/polyether sulfone composite for selective laser sintering. *3D Printing and Additive Manufacturing, 26*. DOI 10.1089/3dp.2021.0036.
22. Yu, Y. Q., Guo, Y. L., Jiang, K. Y., Li, J., Guo, D. (2017). Laser sintering and post-processing of a walnut shell/Co-PES composite. *RSC Advances, 7(37),* 23176–23181. DOI 10.1039/C7RA00775B.
23. Zhao, S., Yang, Z., Zhou, X. G., Ling, X. Z., Mora, L. S. et al. (2014). Design, fabrication, characterization and simulation of PIp-SiC/SiC composites. *Computers, Materials & Continua, 42(2),* 103–124. DOI 10.3970/cmc.2014.042.103.

24. Bilal, A., Van, D., Fitzpatrick, M. E., Hua, G. (2018). Residual stress evaluation in selective-laser-melting additively manufactured titanium (Ti-6Al-4V) and inconel 718 using the contour method and numerical simulation. *Additive Manufacturing, 22(8),* 571–582. DOI 10.1016/j.addma.2018.06.002.
25. Ma, R. L., Peng, C. Q., Cai, Z. Y., Wang, R. C., Zhou, Z. H. et al. (2021). Finite element analysis of temperature and stress fields during selective laser melting process of Al-Mg-Sc-Zr alloy. *Transactions of Nonferrous Metals Society of China, 31(10),* 2922–2938. DOI 10.1016/S1003-6326(21)65703-5.
26. Yu, B. Y., He, L., Zheng, L., Yu, B. N., Long, Y. L. (2020). Numerical Simulation and Microstructure analysis of residual stress in SLM formed AlSi10Mg. *Special Casting & Nonferrous Alloys, 40(4),* 349–355. DOI 10.15980/j.tzzz.2020.04.00.
27. Liang, H., Ren, A. (2001). Study on thermal stress field in polymer-coated ceramic powder products sintering. *Ordnance Material Science and Engineering, (3),* 35–37.
28. Li, J., Yuan, S., Zhu, J., Li, S., Zhang, W. (2020). Numerical model and experimental validation for laser sinterable semi-crystalline polymer: Shrinkage and warping. *Polymers, 12(6),* 1373. DOI 10.3390/polym12061373.
29. Cai, L. L., Ding, H. L., Meng, J., Wen, X., Yan, B. (2021). Warping simulation of selective laser sintering. *Die and Mould Technology, 12(2),* 44–50.
30. Yu, Y. Q., Jiang, M. Z., Wang, S. L., Guo, Y. L., Jiang, T. et al. (2021). Dynamic evolution simulation of sintering pool in selective laser sintering walnut shell/Co-PES composite. *Optics & Laser Technology, 144(1–4),* 107425. DOI 10.1016/j.optlastec.2021.107425.
31. Riedlbauer, D., Drexler, M., Drummer, D., Steinmann, P., Mergheim, J. (2014). Modelling, simulation and experimental validation of heat transfer in selective laser melting of the polymeric material Pa12. *Computational Materials Science, 93(10),* 239–248. DOI 10.1016/j.commatsci.2014.06.046.